DOI: 10.3901/CJME.2015.1210.144, available online at www.springerlink.com; www.cjmenet.com

Accuracy Analysis and Design of A3 Parallel Spindle Head

NI Yanbing[1,*], ZHANG Biao[1], SUN Yupeng[2], and ZHANG Yuan[1]

1 *School of Mechanical Engineering, Tianjin University, Tianjin 300072, China*
2 *China Faw Group Corporation R&D Center, Changchun 130000, China*

Received August 11, 2015; revised November 23, 2015; accepted December 10, 2015

Abstract: As functional components of machine tools, parallel mechanisms are widely used in high efficiency machining of aviation components, and accuracy is one of the critical technical indexes. Lots of researchers have focused on the accuracy problem of parallel mechanisms, but in terms of controlling the errors and improving the accuracy in the stage of design and manufacturing, further efforts are required. Aiming at the accuracy design of a 3-DOF parallel spindle head(A3 head), its error model, sensitivity analysis and tolerance allocation are investigated. Based on the inverse kinematic analysis, the error model of A3 head is established by using the first-order perturbation theory and vector chain method. According to the mapping property of motion and constraint Jacobian matrix, the compensatable and uncompensatable error sources which affect the accuracy in the end-effector are separated. Furthermore, sensitivity analysis is performed on the uncompensatable error sources. The sensitivity probabilistic model is established and the global sensitivity index is proposed to analyze the influence of the uncompensatable error sources on the accuracy in the end-effector of the mechanism. The results show that orientation error sources have bigger effect on the accuracy in the end-effector. Based upon the sensitivity analysis results, the tolerance design is converted into the issue of nonlinearly constrained optimization with the manufacturing cost minimum being the optimization objective. By utilizing the genetic algorithm, the allocation of the tolerances on each component is finally determined. According to the tolerance allocation results, the tolerance ranges of ten kinds of geometric error sources are obtained. These research achievements can provide fundamental guidelines for component manufacturing and assembly of this kind of parallel mechanisms.

Keywords: A3 head, error model, sensitivity analysis, tolerance allocation

1 Introduction

With the advantages of high-speed, high accuracy and good dynamic performance, parallel mechanisms have been widely used in aviation and aerospace industry, such as Tricept module[1–2], Exechon hybrid module[3], Sprint Z3[4] and so on. Sprint Z3, designed by DS-Technology Company, has been widely used in the high-speed milling for the large scale structural components. In China, based on the 3-RPS mechanism, Tianjin University developed a novel 3-DOF parallel mechanism named A3 head[5], which had one translation and two rotations. As functional component, the A3 head can be combined with traditional X/Y workbench to build a 5-axis high-speeding machining center for high-speed machining of large structural components. For the above machine tools application to industry, geometric accuracy is critical.

Generally, the accuracy design of parallel mechanism is twofold, error source analysis and tolerance allocation. The error source analysis focuses on predicting the position and orientation errors of tools in the entire workspace based on the given tolerances of the components, and the bigger effect on pose errors in the end-effector of the mechanism are captured by means of sensitivity analysis. Tolerance allocation is constructing objective function with certain optimized index, and after optimizing tolerance, the tolerance values of each link of parallel mechanism can be obtained. A3 head is a lower mobility parallel mechanism and only the pose errors corresponding to the given degrees of freedom can be compensated by kinematics calibration[6–7]. Thus, the compensatable and uncompensatable error sources which affect the accuracy in the end-effector should be separated. The uncompensatable error sources should be strictly controlled in the stages of design and manufacturing through accuracy design[8].

In recent years, a large number of scholars have studied on the accuracy design of parallel mechanisms. In 1997, based on the space vector chain method, PATEL, et al[9], established the error model of a parallel mechanism, and studied the influence of each error source on the pose accuracy in the end-effector through sensitivity analysis. Using the same method, HUANG, et al[10], established the error model of a parallel mechanism with parallelogram

* Corresponding author. E-mail: niyb5812@tju.edu.cn
Supported by National Natural Science Foundation of China(Grant No. 51575385)

struts structure, and the pose accuracy in the end-effector can be estimated by the analysis result of sensitivity probability model. In 2004, based on a 3-PRS parallel mechanism, WANG, et al[11], developed an error model with 18 errors including hinge joint errors of revolute pair and spherical joint as well as zero errors of prismatic pair, but ignoring the straightness errors of guideway and orientation errors of revolute pair. Founded on this study, O'BRIEN, et al[12], considered the straightness errors of guideway, but ignored the position errors of spherical joint. In 2005, PENG, et al[13], proposed an error modeling approach for parallel mechanism, which can eliminate the influence of systematic error caused by pose parameters on the accuracy of parallel mechanism. In 2006, HUANG, et al[14], studied the tolerance design and optimization of a 2-DOF parallel mechanism, and the effectiveness of the proposed approach was verified by simulation and experiment. In 2009, CHANAL, et al[15], took a five-axis hybrid machine tool as the research objective and analyzed the influence of hinge position on the tolerance design of manufacturing and assembling of each link. In 2011, by utilizing the screw theory, LIU, et al[16], proposed a general error model method, which can be applied on low mobility parallel mechanisms. In the same year, LI, et al[17], studied the accuracy design and accuracy synthesis of a 3-RPS mechanism using the orthogonal design method. Their study can clearly analyze the influence degree of pose parameters on pose errors. In 2013, XIE, et al[18], took a novel virtual center parallel mechanism as research objective and studied the sensitivity analysis of error sources. Through the results, the influence degree of each geometric parameter on the output accuracy of the parallel mechanism was obtained. In the same year, YAO, et al[19], established the error model of Stewart platform and presented the solution methods for the terminal errors of the mechanism based on interval analysis method, which was an effective accuracy analysis method for Stewart platform. In 2014, CHEN, et al[20], proposed an error model of a parallel robot with parallelogram structures, which could disclose the process of error transmission in detail. Based on the error model, the sensitivity analysis was performed to identify the sensitive geometric errors and sensitive areas. In 2015, RUGBANI, et al[21], put forward a novel micro-CMM based on parallel mechanism and established its error model using covariance matrix theory. Also, the effect of geometric errors on probe position was analyzed. The above achievements are quite important to accuracy design of parallel mechanisms, but in terms of improving the accuracy, further efforts are required.

The purpose of this paper is to improve the accuracy of A3 head in the stages of design and manufacturing. First, the inverse kinematics of A3 head is analyzed and the error mapping model is established by perturbation theory. By obtaining the mapping relation of motion and constraint Jacobian matrix, the compensatable and uncompensatable error sources can be separated. Then, the sensitivity analysis is used to analyze the influence of the uncompensatable error sources on the accuracy in the end-effector of the mechanism. Based on the analysis result, the mathematical model is established with the consideration of manufacturing cost. Finally，the tolerance allocation is performed by genetic algorithm. As per the error model, sensitivity analysis and tolerance allocation study, this paper can help the design of A3 head improve its accuracy.

2 Kinematics Analysis

2.1 Mechanism description

As shown in Fig. 1, the topological structure A3 head is a 3-RPS parallel mechanism, which consists of a moving platform(including motorized spindle), a fixed platform and three chains. Each chain contains a R-revolute pair, a P-prismatic pair and a S-spherical joint. Each chain has two ends and one end is connected to fixed platform by revolute pair which is driven by servo motor through screw-nut, and the other end is connected to moving platform by spherical joint.

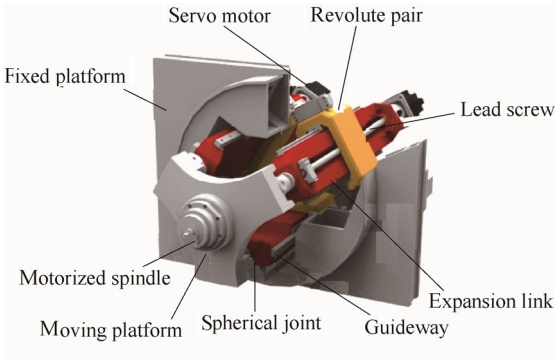

Fig. 1.　Solid model of A3 head

2.2 Inverse kinematic analysis

The schematic diagram of A3 head is shown in Fig. 2. A_i and B_i are the geometrical center of revolute pair R and spherical joint S in each chain, respectively; $\boldsymbol{w}_i$ is the direction vector of each chain, also it can be seen as the direction vector of $\boldsymbol{A}_i\boldsymbol{B}_i$; $\boldsymbol{u}_i$ is the direction vector of each revolute pair axis, which is perpendicular to $\boldsymbol{A}_i\boldsymbol{B}_i$; P is the tool reference point, which is located on the end face of the spindle.

The fixed coordinate system $\{O\}$ is established on the geometrical center point O of the fixed platform, as a result z axis is perpendicular to the plane of fixed platform, x axis positive direction is complying with the vector of A_3A_2, y axis is defined by the right-hand rule(in a three-dimensional coordinate system, thumb is x positive direction, index finger is y positive direction and middle finger is z positive direction). The connected coordinate system $\{O'\}$ is placed on the center point O' of moving platform, where z' axis is perpendicular to the plane of moving platform, x' axis positive direction is consistent with the vector of $\boldsymbol{B}_2\boldsymbol{B}_3$,

y' axis is defined by the right-hand rule.

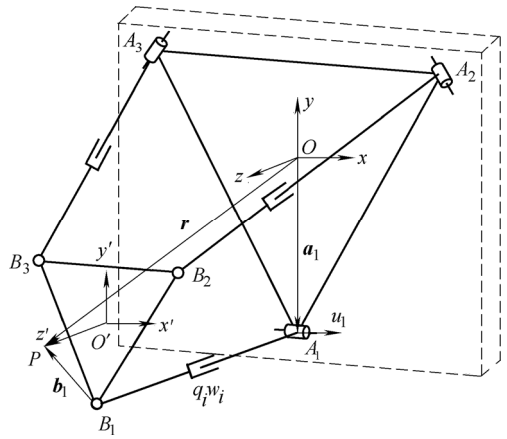

Fig. 2. Schematic diagram of A3

The inverse kinematics of A3 solves for the inputs of three prismatic pairs q_i under the condition of giving the six poses information in the end-effector. The closed-loop constraint equation of this mechanism can be written as

$$\boldsymbol{r} = \boldsymbol{a}_i + q_i\boldsymbol{w}_i + \boldsymbol{R}\boldsymbol{b}_i, \quad i = 1, 2, 3, \tag{1}$$

where $\boldsymbol{r}$ is the distance between geometrical center point O of the fixed platform and tool reference point P; $\boldsymbol{a}_i$ is the distance between point O and the geometrical center of revolute pair; $\boldsymbol{b}_i$ is the distance between point P and the geometrical center of spherical joint.

Since the prismatic pairs of the chains are not able to move along u_i, taking the dot product with u_i^{T} on both sides of the closed-loop equation, the constraint equation can be established as

$$\boldsymbol{u}_i^{\mathrm{T}}\left(\boldsymbol{r} - \boldsymbol{R}\boldsymbol{b}_i\right) = 0, \quad i = 1, 2, 3, \tag{2}$$

where $\boldsymbol{u}_i = \begin{pmatrix}\cos\alpha_i & \sin\alpha_i & 0\end{pmatrix}^{\mathrm{T}}$.

Thus, in Eq. (1), only three linear inputs are unknown. Uniting Eq. (1) and Eq. (2) leads to

$$q_i = \left\|\boldsymbol{a}_i + \boldsymbol{R}\boldsymbol{b}_i - \boldsymbol{r}\right\|, \quad i = 1, 2, 3. \tag{3}$$

The unit direction vector of linear chain can be obtained by q_i as follows:

$$\boldsymbol{w}_i = \frac{\boldsymbol{a}_i + \boldsymbol{R}\boldsymbol{b}_i - \boldsymbol{r}}{q_i}, \quad i = 1, 2, 3. \tag{4}$$

3 Error Modeling

3.1 System description

In order to measure each error source in the unified framework, the coordinate systems can be defined per Fig. 3 as follows.

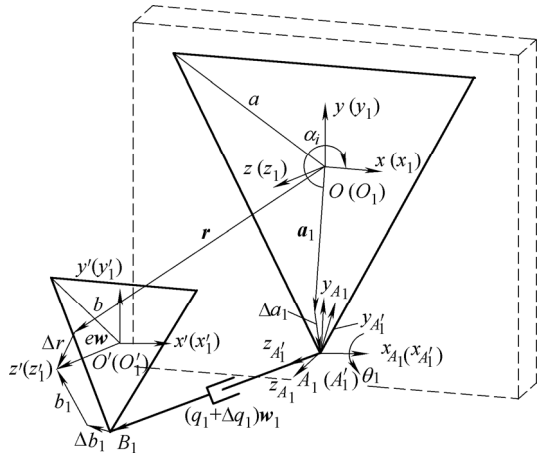

Fig. 3. Schematic diagram of A3 chains with errors

(1) The fixed coordinate system $\{O\}$ of the fixed platform: the origin O is located on the geometrical center of the fixed platform, z axis is perpendicular to the plane of fixed platform, x axis is located in the plane of fixed platform and is parallel to the horizontal plane, y axis is defined by the right-hand rule, and the circumradius of fixed platform is a.

(2) The reference coordinate system $\{O_i\}$ of each chain: the angle of $\{O_i\}$ relative to coordinate system $\{O\}$ is α_i through z axis.

(3) The fixed coordinate system $\{A_i\}$ of revolute pairs: the origin A_i is located on the geometrical center of the revolute pairs, the direction of each axis is similar to coordinate system $\{O_i\}$. In $\{O_i\}$, the nominal position and error vector of origin A_i is $\boldsymbol{a}_i$ and $\Delta\boldsymbol{a}_i$, the orientation error vector of $\{A_i\}$ is $\boldsymbol{\theta}_{A_i}$.

(4) The connected coordinate system $\{A'_i\}$ of prismatic pairs: the origin A'_i is located on the geometrical center of the revolute pairs, $z_{A'_i}$ axis is along the direction of prismatic pair in each chain, the direction of $x_{A'_i}$ axis is similar to x_{A_i}, $y_{A'_i}$ axis is defined by the right-hand rule, and θ_i is the angle of revolute pair. In $\{A_i\}$, the orientation error vector of $\{A'_i\}$ referenced to $\{A_i\}$ is $\boldsymbol{\theta}_{A'_i}$.

(5) The connected coordinate system $\{O'\}$ of moving platform: the origin O' is located on the geometrical center of the moving platform, z' axis is perpendicular to the plane of moving platform, x' axis is parallel to the line of centers of the two spherical joints, y' axis is defined by the right-hand rule, the circumradius of fixed platform is b, $e\boldsymbol{w}$ is the reference cutter location vector, the nominal position and error vector of point O' is $\boldsymbol{r}$ and $\Delta\boldsymbol{r}$, the orientation error vector of $\{O'\}$ referenced to $\{O\}$ is $\boldsymbol{\theta}$.

(6) The reference coordinate system $\{O'_i\}$ of each chain of moving platform: the angle of $\{O'_i\}$ relative to coordinate system $\{O'\}$ is α_i through z' axis. In $\{O'_i\}$, the nominal position and error vector of point B_i referenced to tool nose point is $\boldsymbol{b}_i$ and $\Delta\boldsymbol{b}_i$.

Besides, the nominal position vector and zero error of prismatic pair in each chain is $q_i\boldsymbol{w}_i$ and Δq_i.

Ignoring the spherical joint error, all possible geometric errors of the mechanism are considered and are shown in Table 1.

Table 1. Geometric error sources of A3 head

Geometric error source	Meaning	Remark
$\Delta \boldsymbol{a}_i$	Position errors of point A_i referenced to point O	in $\{O_i\}$
$\Delta \boldsymbol{b}_i$	Position errors of point B_i referenced to point O'	in $\{O_i'\}$
Δq_i	Zero errors	
$\boldsymbol{\theta}_{A_i}$	Orientation errors of $\{A_i\}$ referenced to $\{O_i\}$	in $\{O_i\}$
$\boldsymbol{\theta}_{A_i'}$	Orientation errors of $\{A_i'\}$ referenced to $\{A_i\}$	in $\{A_i\}$

3.2 Error model

Error model is established based on the theory of small perturbation. Taking the perturbation of the position vector equation of tool nose point in the end-effector leads to

$$\begin{aligned}\boldsymbol{r}+\Delta\boldsymbol{r}=&\left[\boldsymbol{E}_3+\boldsymbol{\theta}\times\right]\boldsymbol{R}\boldsymbol{R}_i\left(\boldsymbol{b}+\Delta\boldsymbol{b}_i\right)+\boldsymbol{R}_i\left(\boldsymbol{a}+\Delta\boldsymbol{a}_i\right)+\\&\boldsymbol{R}_i\left[\boldsymbol{E}_3+\boldsymbol{\theta}_{A_i}\times\right]\boldsymbol{R}_{A_i'}\left[\boldsymbol{E}_3+\boldsymbol{\theta}_{A_i'}\times\right]\left(q_i+\Delta q_i\right)\boldsymbol{e}_3,\end{aligned}\tag{5}$$

where

$$\boldsymbol{e}_3=(0\quad 0\quad 1)^{\mathrm{T}},\ i=1,2,3,\ \boldsymbol{E}_3=\begin{pmatrix}1&0&0\\0&1&0\\0&0&1\end{pmatrix},$$

$$\boldsymbol{R}_i=\begin{pmatrix}\cos\alpha_i&-\sin\alpha_i&0\\\sin\alpha_i&\cos\alpha_i&0\\0&0&1\end{pmatrix},\quad \boldsymbol{R}_{A_i'}=\begin{pmatrix}1&0&0\\0&\cos\theta_i&-\sin\theta_i\\0&\sin\theta_i&\cos\theta_i\end{pmatrix}.$$

$\boldsymbol{\theta}_{A_i}\times$, $\boldsymbol{\theta}_{A_i'}\times$, $\boldsymbol{\theta}\times$ is the antisymmetric representation of orientation error vector $\boldsymbol{\theta}_{A_i}$, $\boldsymbol{\theta}_{A_i'}$, $\boldsymbol{\theta}$. The antisymmetric representation of vector is the first order tensor, which can do multiplication cross operation. Taking $\boldsymbol{\theta}\times$ as an example, when $\boldsymbol{\theta}=\left(\Delta\alpha\quad\Delta\beta\quad\Delta\gamma\right)^{\mathrm{T}}$, then

$$\boldsymbol{\theta}\times=\begin{pmatrix}0&-\Delta\gamma&\Delta\beta\\\Delta\gamma&0&-\Delta\alpha\\-\Delta\beta&\Delta\alpha&0\end{pmatrix}.$$

Taking linearization of Eq. (5) and taking subtraction of it and nominal position vector of tool nose point leads to

$$\begin{aligned}\Delta\boldsymbol{r}=&\boldsymbol{R}_i\Delta\boldsymbol{a}_i+\Delta q_i\boldsymbol{w}_i+q_i\left(\boldsymbol{R}_i\boldsymbol{R}_{A_i'}\boldsymbol{\theta}_{A_i'}\right)\times\boldsymbol{w}_i+\\&\left(q_i\boldsymbol{R}_i\boldsymbol{\theta}_{A_i}\right)\times\boldsymbol{w}_i+\boldsymbol{R}\boldsymbol{R}_i\Delta\boldsymbol{b}_i+\boldsymbol{\theta}\times\left(\boldsymbol{R}\boldsymbol{b}_i\right),\end{aligned}\tag{6}$$

where $\boldsymbol{w}_i=\boldsymbol{R}_i\boldsymbol{R}_{A_i'}\boldsymbol{e}_3$, $\boldsymbol{b}_i=\boldsymbol{R}_i\boldsymbol{b}$.

Taking the dot product with $\boldsymbol{w}_i^{\mathrm{T}}$ on both sides of Eq. (6) and moving pose error in the end-effector to the left side of the equation leads to

$$\boldsymbol{w}_i^{\mathrm{T}}\Delta\boldsymbol{r}=\boldsymbol{w}_i^{\mathrm{T}}\boldsymbol{R}_i\Delta\boldsymbol{a}_i+\Delta q_i+\boldsymbol{w}_i^{\mathrm{T}}\boldsymbol{R}\boldsymbol{R}_i\Delta\boldsymbol{b}_i+\left[\left(\boldsymbol{R}\boldsymbol{b}_i\right)\times\boldsymbol{w}_i\right]^{\mathrm{T}}\Delta\boldsymbol{\theta}.\tag{7}$$

Taking the dot product with $\boldsymbol{u}_i^{\mathrm{T}}$ on both sides of Eq. (6) and moving pose error in the end-effector to the left side of the equation leads to

$$\begin{aligned}\boldsymbol{u}_i^{\mathrm{T}}\Delta\boldsymbol{r}=&q_i\left(\boldsymbol{w}_i\times\boldsymbol{u}_i\right)^{\mathrm{T}}\boldsymbol{R}_i\boldsymbol{R}_{A_i'}\boldsymbol{\theta}_{A_i'}+q_i\left(\boldsymbol{w}_i\times\boldsymbol{u}_i\right)^{\mathrm{T}}\boldsymbol{R}_i\boldsymbol{\theta}_{A_i}+\\&\boldsymbol{u}_i^{\mathrm{T}}\boldsymbol{R}_i\Delta\boldsymbol{a}_i+\boldsymbol{u}_i^{\mathrm{T}}\boldsymbol{R}\boldsymbol{R}_i\Delta\boldsymbol{b}_i+\left[\left(\boldsymbol{R}\boldsymbol{b}_i\right)\times\boldsymbol{u}_i\right]^{\mathrm{T}}\Delta\boldsymbol{\theta}.\end{aligned}\tag{8}$$

Rewriting and simplifying Eq. (7) and Eq. (8) in matrix form yields

$$\boldsymbol{J}\Delta\boldsymbol{x}=\boldsymbol{N}\Delta\boldsymbol{\varepsilon},\tag{9}$$

where

$$\Delta\boldsymbol{x}=\begin{pmatrix}\Delta\boldsymbol{r}\\\Delta\boldsymbol{\theta}\end{pmatrix},\quad \boldsymbol{J}=\begin{pmatrix}\boldsymbol{J}_a\\\boldsymbol{J}_c\end{pmatrix},\quad \boldsymbol{N}=\begin{pmatrix}\boldsymbol{N}_a&\boldsymbol{0}\\\boldsymbol{0}&\boldsymbol{N}_c\end{pmatrix},$$

$$\boldsymbol{J}_a=\begin{pmatrix}\boldsymbol{w}_1^{\mathrm{T}}&-\left(\boldsymbol{R}\boldsymbol{b}_i\times\boldsymbol{w}_1\right)^{\mathrm{T}}\\\boldsymbol{w}_2^{\mathrm{T}}&-\left(\boldsymbol{R}\boldsymbol{b}_i\times\boldsymbol{w}_2\right)^{\mathrm{T}}\\\boldsymbol{w}_3^{\mathrm{T}}&-\left(\boldsymbol{R}\boldsymbol{b}_i\times\boldsymbol{w}_3\right)^{\mathrm{T}}\end{pmatrix},\quad \boldsymbol{J}_c=\begin{pmatrix}\boldsymbol{u}_1^{\mathrm{T}}&-\left(\boldsymbol{R}\boldsymbol{b}_i\times\boldsymbol{u}_1\right)^{\mathrm{T}}\\\boldsymbol{u}_2^{\mathrm{T}}&-\left(\boldsymbol{R}\boldsymbol{b}_i\times\boldsymbol{u}_2\right)^{\mathrm{T}}\\\boldsymbol{u}_3^{\mathrm{T}}&-\left(\boldsymbol{R}\boldsymbol{b}_i\times\boldsymbol{u}_3\right)^{\mathrm{T}}\end{pmatrix},$$

$$\boldsymbol{N}_a=\operatorname{diag}\left(\boldsymbol{N}_{a_i}\right),\quad \boldsymbol{N}_c=\operatorname{diag}\left(\boldsymbol{N}_{c_i}\right),$$

$$\boldsymbol{N}_{a_i}=\left(\sin\theta_i\quad\cos\theta_i\quad 1\quad\boldsymbol{w}_i^{\mathrm{T}}\boldsymbol{R}\boldsymbol{R}_i\right),$$

$$\boldsymbol{N}_{c_i}=\left(1\quad q_i(\boldsymbol{w}_i\times\boldsymbol{u}_i)^{\mathrm{T}}\boldsymbol{R}_i\boldsymbol{R}_{A_i'}\quad q_i(\boldsymbol{w}_i\times\boldsymbol{u}_i)^{\mathrm{T}}\boldsymbol{R}_i\quad\boldsymbol{u}_i^{\mathrm{T}}\boldsymbol{R}\boldsymbol{R}_i\right),$$

$$\Delta\boldsymbol{\varepsilon}_p=\left(\Delta\boldsymbol{\varepsilon}_{a_1}^{\mathrm{T}}\quad\Delta\boldsymbol{\varepsilon}_{a_2}^{\mathrm{T}}\quad\Delta\boldsymbol{\varepsilon}_{a_3}^{\mathrm{T}}\quad\Delta\boldsymbol{\varepsilon}_{c_1}^{\mathrm{T}}\quad\Delta\boldsymbol{\varepsilon}_{c_2}^{\mathrm{T}}\quad\Delta\boldsymbol{\varepsilon}_{c_3}^{\mathrm{T}}\right)^{\mathrm{T}},$$

$$\Delta\boldsymbol{\varepsilon}_{a_i}=\left(\Delta a_{iy}\quad\Delta a_{iz}\quad\Delta q_i\quad\Delta\boldsymbol{b}_i^{\mathrm{T}}\right)^{\mathrm{T}},$$

$$\Delta\boldsymbol{\varepsilon}_{c_i}=\left(\Delta a_{ix}\quad\boldsymbol{\theta}_{A_i'}^{\mathrm{T}}\quad\boldsymbol{\theta}_{A_i}^{\mathrm{T}}\quad\Delta\boldsymbol{b}_i^{\mathrm{T}}\right)^{\mathrm{T}},$$

where $\boldsymbol{J}_a$ and $\boldsymbol{J}_c$ is respectively the driving Jacobian matrix and constraint Jacobian matrix, and the pose errors $\Delta\boldsymbol{x}$ in the end-effector can be mapped into two kinds of errors by $\boldsymbol{J}_a$ and $\boldsymbol{J}_c$. Since the driving Jacobian matrix $\boldsymbol{J}_a$ is the mapping operator in the motion space of the mechanism, the geometric error sources which are mapped into this space are compensatable errors. Since the constraint Jacobian matrix $\boldsymbol{J}_c$ is the mapping operator in the constraint space of the mechanism, the geometric error sources which are mapped into this space are uncompensatable errors.

So far, all the compensatable error sources $\Delta\boldsymbol{\varepsilon}_{a_i}$ and uncompensatable error sources $\Delta\boldsymbol{\varepsilon}_{c_i}$ of A3 head are obtained by error model and error separation. There are 18 compensatable error sources which are the components Δa_{iy} and Δa_{iz} of position errors $\Delta\boldsymbol{a}_i$ along y_i and z_i axis in $\{O_i\}$, zero errors Δq_i and position errors $\Delta\boldsymbol{b}_i$, and these geometric errors can be compensated by kinematic calibration. And there are 30 uncompensatable error sources which are the components Δa_{ix} of position errors $\Delta\boldsymbol{a}_i$ along x_i axis in $\{O_i\}$, orientation errors $\boldsymbol{\theta}_{A_i}$ and $\boldsymbol{\theta}_{A_i'}$, and

position errors $\Delta \boldsymbol{b}_i$, and these geometric errors should be controlled in the process of manufacturing and assembling. Since the existence of carrier motion in A3 head, there are common errors which are Δb_{ix}, Δb_{iy} and Δb_{iz} in the compensatable and uncompensatable error sources.

4 Sensitivity Analysis

Sensitivity analysis is performed on the uncompensatable error sources. In terms of the statistical significance, through the investigation of the influence of uncompensatable errors on the position and orientation accuracy in the end-effector, the sensitivity probabilistic model is established and its general form is obtained as

$$\Delta \boldsymbol{x} = \boldsymbol{J}_{\varepsilon} \Delta \boldsymbol{\varepsilon}_c , \tag{10}$$

where $\boldsymbol{J}_{\varepsilon} = \boldsymbol{J}^{+} \boldsymbol{N}_c$.

$\Delta \boldsymbol{x}$, $\Delta \boldsymbol{\varepsilon}_c$ and $\boldsymbol{J}_{\varepsilon}$ respectively represents the error vector of tool nose point, the geometric error vector and error Jacobian matrix between them. Partitioning $\boldsymbol{J}_{\varepsilon}$ according to the position and orientation error leads to

$$\boldsymbol{J}_{\varepsilon} = \begin{pmatrix} \boldsymbol{J}_{\varepsilon r} \\ \boldsymbol{J}_{\varepsilon \theta} \end{pmatrix}. \tag{11}$$

Establishing the global sensitivity indexes of volumetric error $\delta_r = \sqrt{\Delta \boldsymbol{r}^{\mathrm{T}} \Delta \boldsymbol{r}}$, squareness error $\delta_\alpha = \sqrt{\Delta\alpha^2 + \Delta\beta^2}$, and angular error $\delta_\phi = \Delta\gamma$ of tool axis, we have

$$\bar{\mu}_{rk} = \left(\int_V \mu_{rk} \mathrm{d}V \right) \Big/ V , \quad \mu_{rk} = \sqrt{\sum_{i=1}^{3} \sum_{m=1}^{3} \boldsymbol{J}_{\varepsilon rimk}^2} ,$$

$$\bar{\mu}_{\alpha k} = \left(\int_V \mu_{\alpha k} \mathrm{d}V \right) \Big/ V , \quad \mu_{\alpha k} = \sqrt{\sum_{i=1}^{3} \sum_{m=1}^{2} \boldsymbol{J}_{\varepsilon \theta imk}^2} ,$$

$$\bar{\mu}_{\phi k} = \left(\int_V \mu_{\phi k} \mathrm{d}V \right) \Big/ V , \quad \mu_{\phi k} = \sqrt{\sum_{i=1}^{3} \sum_{m=3}^{3} \boldsymbol{J}_{\varepsilon \theta imk}^2} ,$$

where V is the volume of the prescribed workspace, $\boldsymbol{J}_{\varepsilon rimk}$ ($\boldsymbol{J}_{\varepsilon \theta imk}$) is the element of row m and column k in $\boldsymbol{J}_{\varepsilon r}$ ($\boldsymbol{J}_{\varepsilon \theta}$) of chain i.

The dimension parameters and workspace of A3 head are shown in Tables 2 and 3.

Table 2. Dimension parameters of A3 head

Dimension parameter/mm	Value
a	250
b	250
e	490

Table 3. Workspace of A3 head

Workspace	Range
Displacement in z direction/m	0.9–1.1
Nutational angle θ/(°)	0–40
Precessional angle ψ/(°)	0–360

Figs. 4–6 show the global sensitivity of volumetric error δ_r, squareness error δ_α and spindle angular error δ_ϕ with respect to the uncompensatable error $\Delta \varepsilon_{ck}'$.

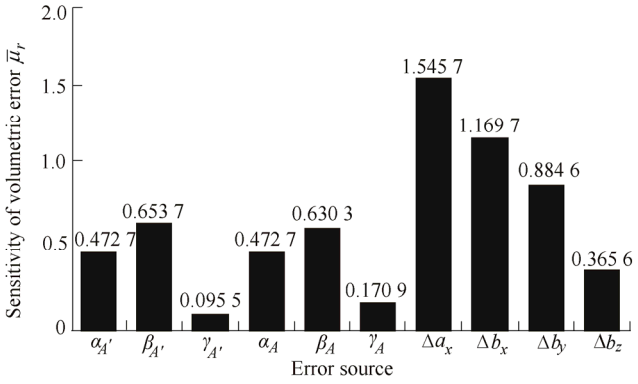

Fig. 4. Sensitivity coefficient of each error source with respect to the volumetric error in the end-effector

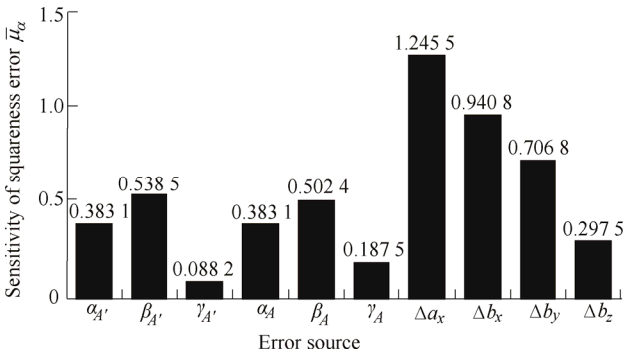

Fig. 5. Sensitivity coefficient of each error source with respect to the squareness error of tool in the end-effector

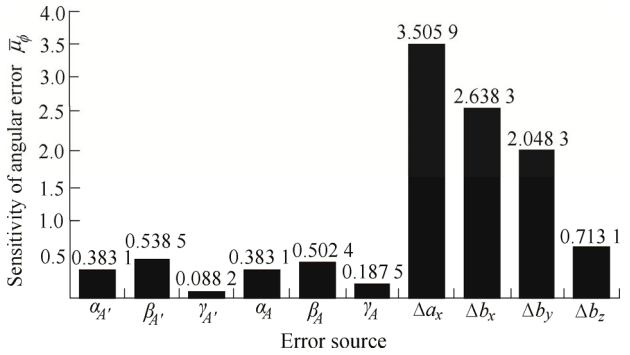

Fig. 6. Sensitivity coefficient of each error source with respect to the angular error of z axis

It can be seen from the figures that volumetric error δ_r is sensitive to the position error Δa_{ix}, Δb_{ix} and orientation error $\alpha_{A_i'}, \beta_{A_i'}, \alpha_{A_i}, \beta_{A_i}$. The influence law of squareness error δ_α in the end-effector on the uncompensatable errors is similar to the volumetric error. As the influence coefficients are high, each error source has big effect on the angular error δ_ϕ of z axis in the end-effector.

The influence law of each uncompensatable error source on the pose errors in the end-effector is different in the workspace. The calculation shows that the influence of

angular errors on pose accuracy in the end-effector increases with the increase of cross section in the workspace, while the influence of position errors on pose accuracy in the end-effector is the same in any cross section in the workspace. Selecting three planes z=0.9 m, z=1.0 m and z=1.1 m in the workspace and taking sensitivity coefficients of angular errors $\boldsymbol{\theta}_{A_i'}$ and position errors $\Delta\boldsymbol{b}_i$ with respect to three errors in the end-effector as examples, the change laws are shown in Figs. 7–15.

The figures show that the change of angular errors $\alpha_{A_i'}$ and $\beta_{A_i'}$ with respect to the two errors in the workspace is relevant to the value of z; the change of $\gamma_{A_i'}$ with respect to the two errors is also relevant to the value of z, but it is not significant; the change of position errors Δb_{ix}, Δb_{iy}, Δb_{iz} is not related to the value of z. In the aspect of change law in working cross sections, the sensitivity coefficient of each error source with respect to the volumetric error and squareness error increases with the increase of $\sqrt{x^2+y^2}$, which means the closer to the boundary of workspace, the more sensitive the errors in the end-effector react, while the sensitivity coefficient of Δb_{ix}, Δb_{iy}, $\alpha_{A_i'}$ and $\beta_{A_i'}$ with respect to the spindle angular error in the end-effector decreases with the increase of $\sqrt{x^2+y^2}$.

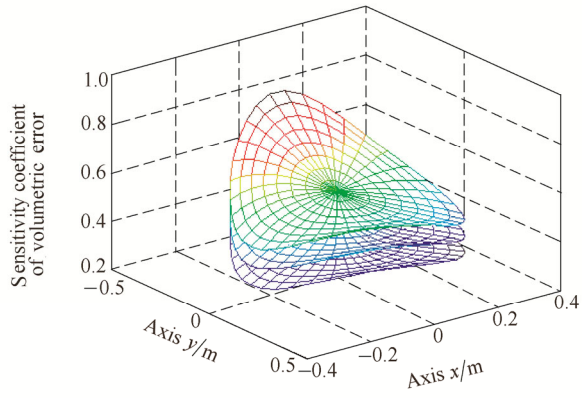

(a) $\alpha_{A_i'}$ with respect to δ_r

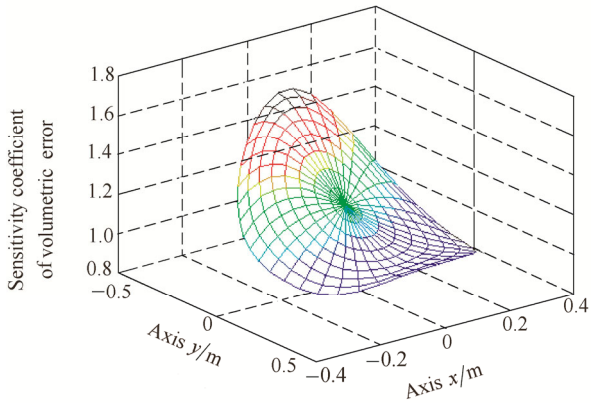

(b) Δb_{ix} with respect to δ_r

Fig. 7. Change law of $\alpha_{A_i'}$ and Δb_{ix} with respect to δ_r in the plane of z=0.9 m, z=1.0 m and z=1.1 m in the workspace

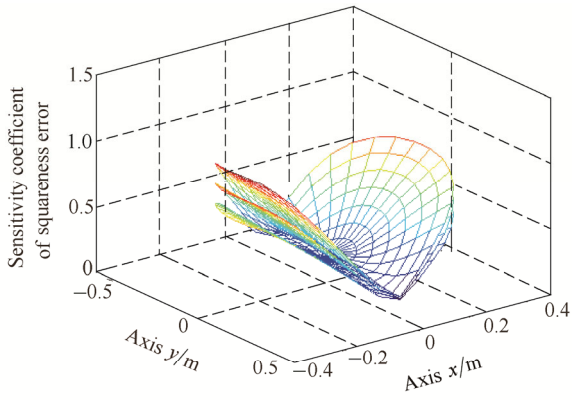

(a) $\alpha_{A_i'}$ with respect to δ_α

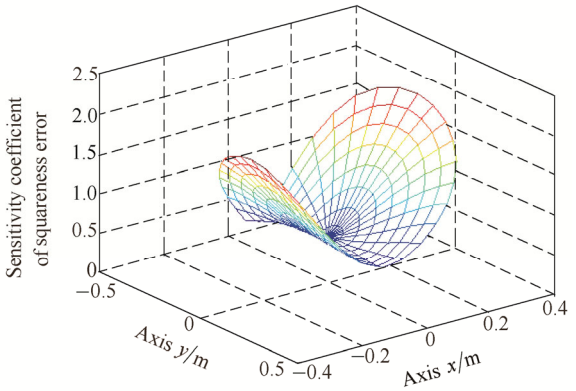

(b) Δb_{ix} with respect to δ_α

Fig. 8. Change law of $\alpha_{A_i'}$ and Δb_{ix} with respect to δ_α in the plane of z=0.9 m, z=1.0 m and z=1.1 m in the workspace

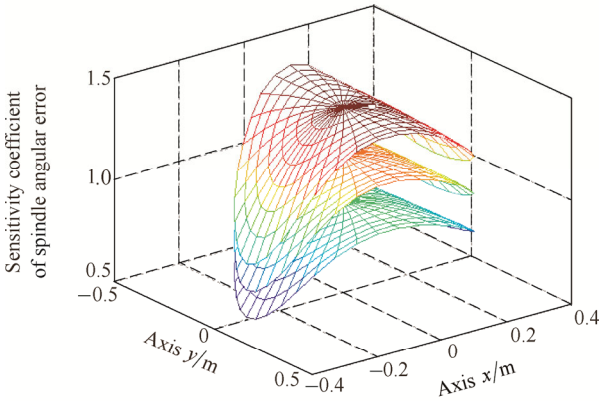

(a) $\alpha_{A_i'}$ with respect to δ_ϕ

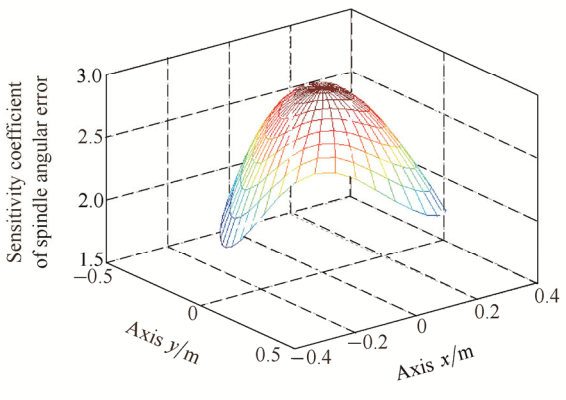

(b) Δb_{ix} with respect to δ_ϕ

Fig. 9. Change law of $\alpha_{A_i'}$ and Δb_{ix} with respect to δ_ϕ in the plane of z=0.9 m, z=1.0 m and z=1.1 m in the workspace

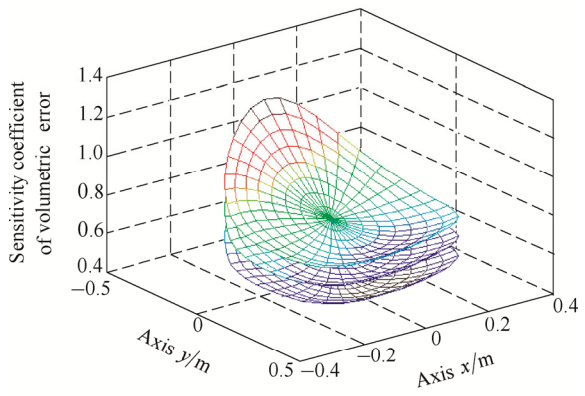

(a) $\beta_{A_i'}$ with respect to δ_r

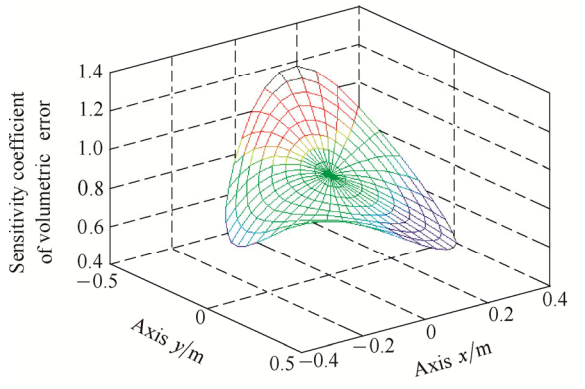

(b) Δb_{iy} with respect to δ_r

Fig. 10. Change law of $\beta_{A_i'}$ and Δb_{iy} with respect to δ_r in the plane of z=0.9 m, z=1.0 m and z=1.1 m in the workspace

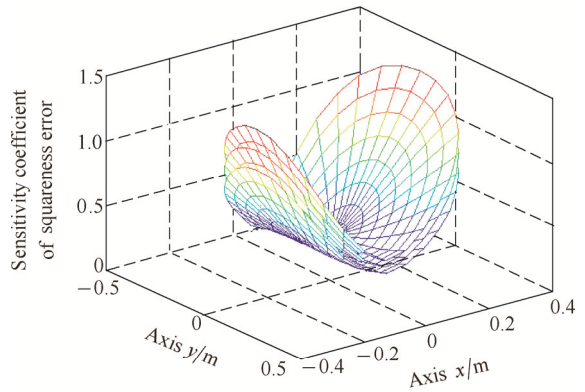

(a) $\beta_{A_i'}$ with respect to δ_α

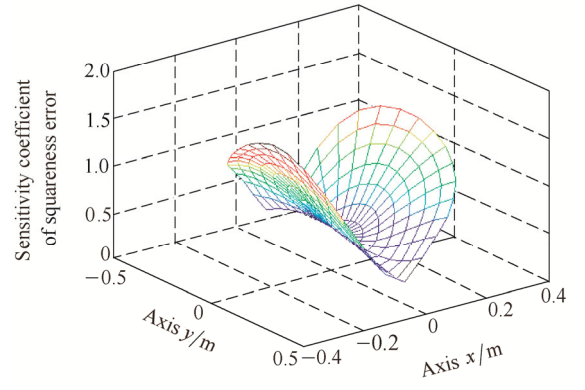

(b) Δb_{iy} with respect to δ_α

Fig. 11. Change law of $\beta_{A_i'}$ and Δb_{iy} with respect to δ_α in the plane of z=0.9 m, z=1.0 m and z=1.1 m in the workspace

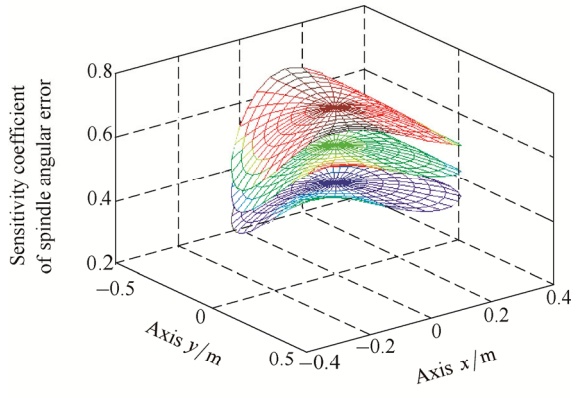

(a) $\beta_{A_i'}$ with respect to δ_ϕ

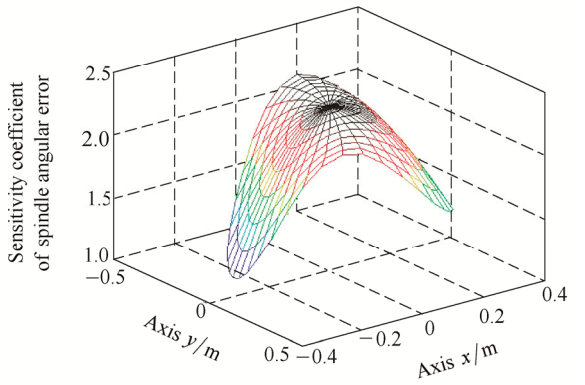

(b) Δb_{iy} with respect to δ_ϕ

Fig. 12. Change law of $\beta_{A_i'}$ and Δb_{iy} with respect to δ_ϕ in the plane of z=0.9 m, z=1.0 m and z=1.1 m in the workspace

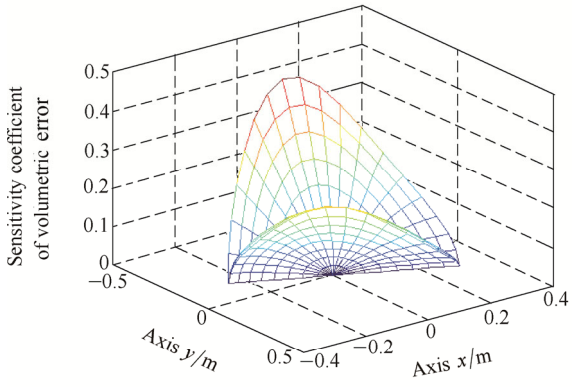

(a) $\gamma_{A_i'}$ with respect to δ_r

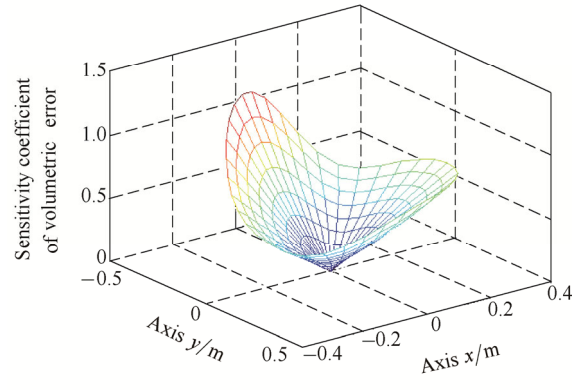

(b) Δb_{iz} with respect to δ_r

Fig. 13. Change law of $\gamma_{A_i'}$ and Δb_{iz} with respect to δ_r in the plane of z=0.9 m, z=1.0 m and z=1.1 m in the workspace

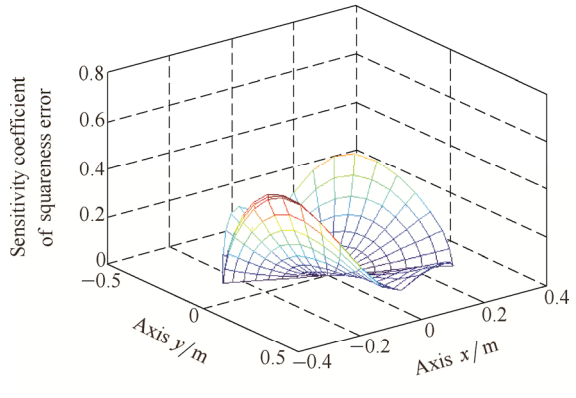

(a) $\gamma_{A_i'}$ with respect to δ_α

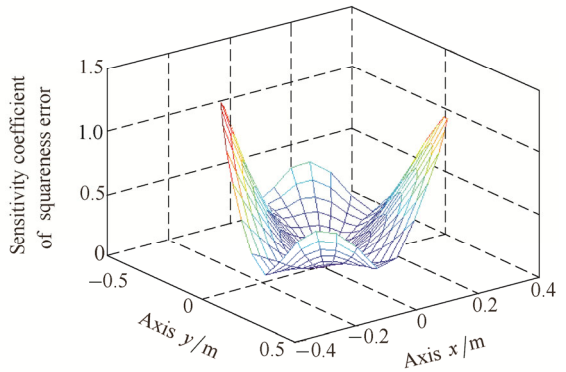

(b) Δb_{iz} with respect to δ_α

Fig. 14. Change law of $\gamma_{A_i'}$ and Δb_{iz} with respect to δ_α in the plane of z=0.9 m, z=1.0 m and z=1.1 m in the workspace

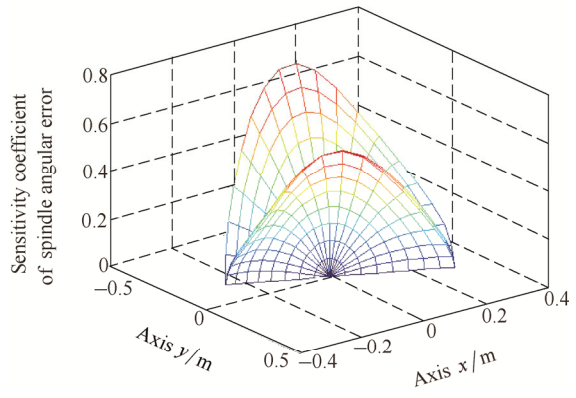

(a) $\gamma_{A_i'}$ with respect to δ_ϕ

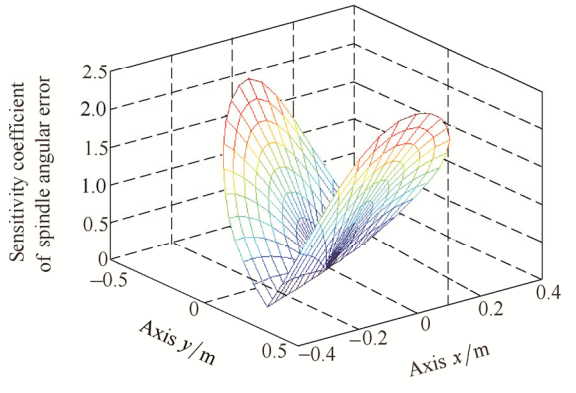

(b) Δb_{iz} with respect to δ_ϕ

Fig. 15. Change law of $\gamma_{A_i'}$ and Δb_{iz} with respect to δ_ϕ in the plane of z=0.9 m, z=1.0 m and z=1.1 m in the workspace

5 Tolerance Allocation

According to the analysis results of last section, tolerance allocation is optimized by calculation. There are ten kinds of geometric error sources which are uncompensatable in each chain of A3 head. In order to reduce the manufacturing cost, the tolerance of geometric parameters should be relaxed as far as possible under the premise of the tolerance of position error δ_r and orientation error $\alpha_{A_i'}$, $\beta_{A_i'}$ being less than the allowable values in the global workspace. Thus, assuming the ten kinds of uncompensatable error sources as design variables, the tolerance manufacturing cost as objective function, and the required tolerance range of three kinds of errors δ_r, δ_α, δ_ϕ and each error source as the constraint factors, the tolerance design of each component is converted into the issue of nonlinearly constrained optimization as follows:

$$\min f = \sum_{k=1}^{10} \frac{s_k}{\sigma^2\left(\Delta\varepsilon_{ck}'\right)}, \quad k = 1-10. \tag{12}$$

Let

$$\begin{cases} \max\left(\sigma\left(\delta_r\right)\right) \leqslant \left[\sigma\left(\delta_r\right)\right], \\ \max\left(\sigma\left(\delta_\alpha\right)\right) \leqslant \left[\sigma\left(\delta_\alpha\right)\right], \\ \max\left(\sigma\left(\delta_\phi\right)\right) \leqslant \left[\sigma\left(\delta_\phi\right)\right], \\ \inf\left(\sigma\left(\Delta\varepsilon_{ck}'\right)\right) \leqslant \sigma\left(\Delta\varepsilon_{ck}'\right) \leqslant \sup\left(\sigma\left(\Delta\varepsilon_{ck}'\right)\right), \end{cases} \tag{13}$$

where s_k is the weight coefficient which is defined by the sensitivity coefficient of each error source; $\max\left(\sigma\left(\delta_r\right)\right)$ is the maximum of standard deviation of volumetric error; $\max\left(\sigma\left(\delta_\alpha\right)\right)$ is the maximum of standard deviation of squareness error in the end-effector; $\max\left(\sigma\left(\delta_\phi\right)\right)$ is the maximum of standard deviation of spindle angular error; $\left[\sigma\left(\delta_r\right)\right]$ is the maximum allowable value of standard deviation of volumetric error; $\left[\sigma\left(\delta_\alpha\right)\right]$ is the maximum allowable value of standard deviation of squareness error in the end-effector; $\left[\sigma\left(\delta_\phi\right)\right]$ is the maximum allowable value of standard deviation of spindle angular error; $\sup\left(\sigma\left(\Delta\varepsilon_{ck}'\right)\right)$ is the upper limit of standard deviation of uncompensatable error sources; $\inf\left(\sigma\left(\Delta\varepsilon_{ck}'\right)\right)$ is the lower limit of standard deviation of uncompensatable error sources.

This is a complicated system optimization problem, which is calculated by genetic algorithm. Genetic algorithm is an optimization method based on the principle of natural evaluation. First, it searches for a set of approximate optimal values in all the possible values, which are formed into genetic population. Then, it screens the satisfactory individuals among the genetic group to form new

population. In the screening process, new individuals are continuously produced by crossover and mutation. Finally, a set of satisfactory optimal values are obtained. Comparing with other optimization methods, genetic algorithm is an efficient, parallel and global searching method and its advantages can be expressed as follows: the universality of feasible solution, the character of population searching, the character of random searching, the high probability of searching global optimal values, and so on[22].

In this problem, the solving process is directly performed by calling the genetic algorithm toolbox of Matlab software application. The minimum value of objective function is fitness function, which is determined by Eq. (12). The constraint conditions are determined by Eq. (13). Table 4 shows the allowable parameter values and the standard deviations are determined per JB/T10792.1—2007[23].

The coefficients of genetic algorithm include variable dimension, generations, population size, mutation probability and crossover probability. Each coefficient of genetic algorithm should be selected appropriately in some ranges, which means it should be neither too big nor too small. In this case, variables are the ten kinds of uncompensatable error sources, so variable dimension is 10. The value of generations is 500, which can obtain good calculated value and has better calculation speed. Population size can directly affect the convergence and computational efficiency of genetic algorithm. Fig. 16 shows the optimization process when population size is set as 20 and 80, both of which have bad convergence.

Table 4. Allowable parameter values

Parameter	Value
$[\sigma(\delta_r)]$ /μm	30/6
$[\sigma(\delta_\alpha)]$ /(μm • m^{-1})	40/6
$[\sigma(\delta_\phi)]$ /(μm • m^{-1})	30/6
$\sup(\sigma(\Delta\varepsilon'_{ck}))$ /μm	60
$\inf(\sigma(\Delta\varepsilon'_{ck}))$ /μm	1

Low crossover probability may make genetic search stagnate, while high crossover probability may result in randomization. Fig. 17 shows the optimization process when crossover probability is set as 0.05 and 0.99.

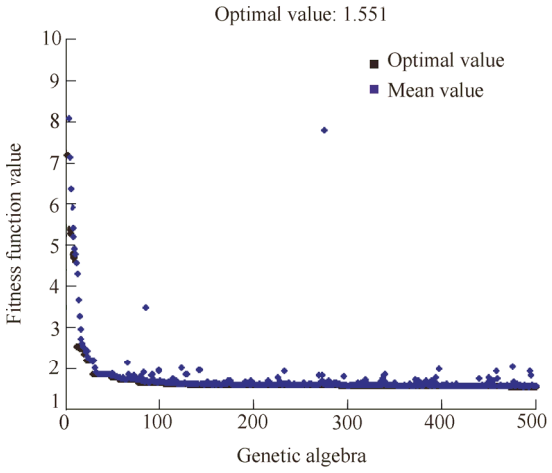

(a) Population size is 20

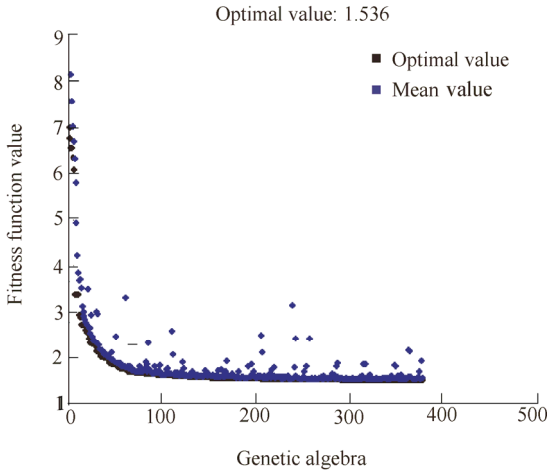

(b) Population size is 80

Fig. 16. Optimization process of fitness function with different population size

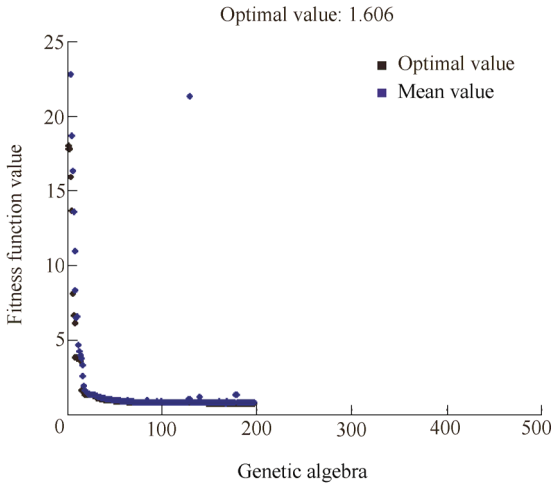

(a) Crossover probabilry is 0.05

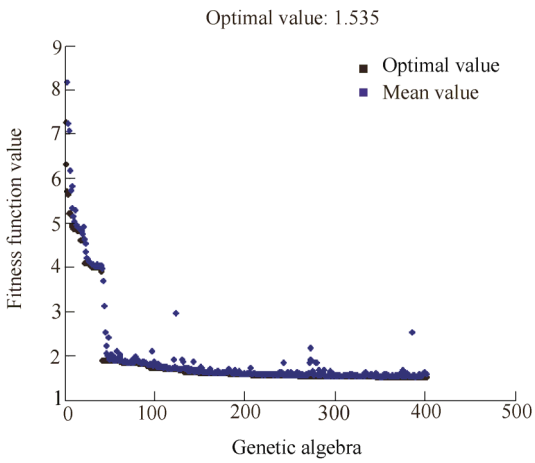

(b) Crossovr probabilry is 0.99

Fig. 17. Optimization process of fitness function with different crossover probability

Mutation probability is also an important factor that affects the genetic search. Low mutation probability may easily generate local extreme value, and high mutation probability also can affect the optimal results. Fig. 18 shows the optimization process when mutation probability is set as 0.001 and 0.08.

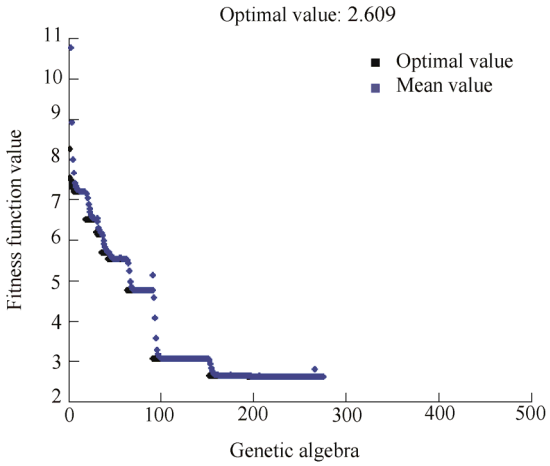

(a) Mutation probability is 0.001

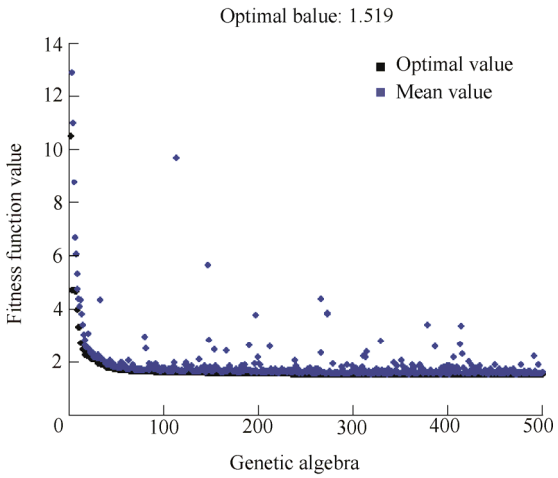

(a) Mutation probability is 0.08

Fig. 18. Optimization process of fitness function with different mutation probability

The above selection process of coefficients just represents some special situations. Actually, a lot of simulations have been done to select the best coefficients. The final coefficients are shown in Table 5. The fitness function values obtained by genetic calculation are shown in Fig. 19.

Table 5. Each coefficient of genetic algorithm

Coefficient	Value
Population size	40
Variable dimension	10
Crossover probability	0.2
Mutation probability	0.025
Generations	500

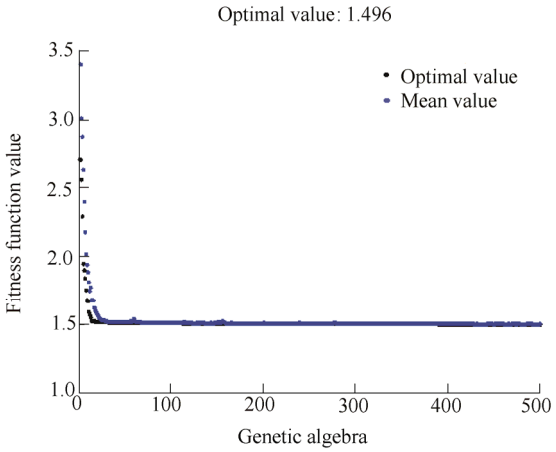

Fig. 19. Optimization process of fitness function

As per the 3σ criterion, the standard deviation of each geometric error source is transformed into the tolerance $T = \pm 3\sigma$, and the results are shown in Table 6.

Table 6. Optimization result of tolerance zone

Tolerance zone	Value
$T(\Delta a_{ix})$ /μm	10
$T(\Delta b_{ix})$ /μm	7
$T(\Delta b_{iy})$ /μm	11
$T(\Delta b_{iz})$ /μm	14
$T(\alpha_{A_i'})$ /(μm • m^{-1})	14
$T(\beta_{A_i'})$ /(μm • m^{-1})	12
$T(\gamma_{A_i'})$ /(μm • m^{-1})	16
$T(\alpha_{A_i})$ /(μm • m^{-1})	15
$T(\beta_{A_i})$ /(μm • m^{-1})	14
$T(\gamma_{A_i})$ /(μm • m^{-1})	16

It must be pointed out that the calculated tolerances are not the manufacturing or assembling tolerances of the components but the tolerance ranges which are required in the stages of manufacturing and assembling. The prototype of A3 parallel spindle head is shown in Fig. 20. According to the measuring results by Renishaw ML10 laser interferometer, when the moving platform is in the center position and moves along z axis in the range of 0–180 mm, the positioning accuracy is 12 μm and the repeated positioning accuracy is 5.8 μm. And according to the measuring results by Renishaw Double Ballbar, the roundness error of the end point is 53.7 μm[24].

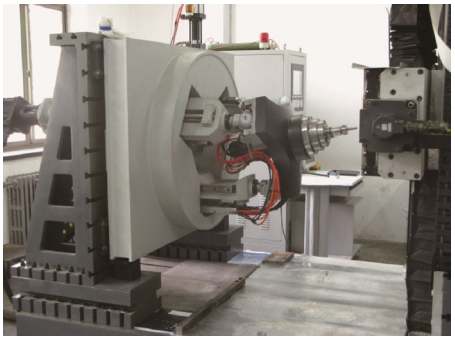

Fig. 20. Prototype of A3 head

6 Conclusions

(1) The error model is established by the perturbation theory and the vector chain method. The compensatable and uncompensatable error sources which affect the A3 head accuracy are separated. There are 18 compensatable error sources and 30 uncompensatable error sources. Since the existence of carrier motion in the mechanism, there are common errors which are Δb_{ix}, Δb_{iy} and Δb_{iz} in the two kinds of error sources.

(2) The sensitivity probabilistic model of uncompensatable error sources is established in terms of the statistical significance, and the global sensitivity indexes are proposed. In addition, the influence of each error source on the pose accuracy in the end-effector is analyzed.

(3) Based on the analysis result, the tolerance allocation of each link is optimized by genetic algorithm and the ten kinds of geometric error sources are obtained, which provide the basis for the manufacturing and assembling of each component.

References

[1] NEUMANN K E. Robot: US, 4732525[P]. 1988-3-22[2015-8-11].

[2] WANG Manxin, WANG Panfeng, SONG Yimin, et al. Stiffness analysis of a 4-DOF hybrid robot[J]. *Journal of Mechanical Engineering*, 2011, 47(15): 9–16. (in Chinese)

[3] JIN Yan, Bi Z M, LIU Haitao, et al. Kinematic analysis and dimensional synthesis of exechon parallel kinematic machine for large volume machining[J]. *Journal of Mechanisms and Robotics*, 2015, 7 (4): 041004-1–041004-8.

[4] WAHL J. Articulated tool head: US, 6431802[P]. 2002-8-13.

[5] HUANG Tian, LIU Haitao. A parallel mechanism with one translation and two rotations: CN, 1843709[P]. 2006-10-11. (in Chinese)

[6] JOUBAIR A, LONG Feizhao, BIGRAS P, et al. Absolute accuracy analysis and improvement of a hybrid 6-DOF medical robot[J]. *Industrial Robot: An International Journal*, 2015, 42(1): 44–53.

[7] CHANG Peng, LI Chengrong, LI Tiemin. Kinematic calibration and forecast error compensation of a 2-DOF planar parallel manipulator[J]. *Chinese Journal of Mechanical Engineering*, 2011, 24(6): 992–998.

[8] LIU Haitao. *Unified parameter modeling of lower mobility robotic manipulators: theory, methodology and application*[D].Tianjin: Tianjin University, 2010. (in Chinese)

[9] PATEL A J, EHMANN K F. Volumetric error analysis of a Stewart platform-based machine tool[J]. *CIRP Annals-Manufacturing Technology*, 1997, 46(1): 287–290.

[10] HUANG Tian, WHITEHOUSE D J, CHETWYND D G. A unified error model for tolerance design, assembly and error compensation of 3-DOF parallel kinematic machines with parallelogram struts[J]. *Annals of CIRP*, 2002, 51(1): 299–303.

[11] WANG H, FAN K. Identification of strut and assembly errors of a 3-PRS serial-parallel machine tool[J]. I*nternational Journal of Machine Tools and Manufacture*, 2004, 44(11): 1171–1178.

[12] O'BRIEN S M, CARRETERO J A, LAST P. Self-calibration of 3-PRS manipulator without redundant sensors[J]. *Transactions of the Canadian Society for Mechanical Engineering*, 2007, 31(4): 483–494.

[13] PENG Binbin, GAO Feng. Modeling for calibration of parallel robot[J]. *Journal of Mechanical Engineering*, 2005, 41(8): 132–135. (in Chinese)

[14] HUANG Tian, CHETWYND D, MEI Jiangping, et al. Tolerance design of a 2-DOF overconstrained translational parallel robot[J]. *IEEE Transactions on Robotics*, 2006, 22(1): 167–172.

[15] CHANAL H, DUC E, RAY P. Reduction of a parallel kinematics machine tool inverse kinematics model with regard to machining behavior[J]. *Mechanism and Machine Theory*, 2009, 44: 1371–1385.

[16] LIU Haitao, HUANG Tian, CHETWYND D G. An approach for error modeling of lower mobility parallel manipulators[J]. *IEEE Transactions on Robotics*, 2012, 3(2): 1–13.

[17] LI Xinyou, CHEN Wuyi, HAN Xianguo. Accuracy analysis and synthesis of 3-RPS parallel machine based on orthogonal design[J]. *Journal of Beijing University of Aeronautics and Astronautics*, 2011, 37(8): 979–984. (in Chinese)

[18] XIE Fugui, LIU Xinjun, CHEN Yuzhen. Error sensitivity analysis of novel virtual center mechanism with parallel kinematics[J]. *Journal of Mechanical Engineering*, 2013, 49(17): 85–91. (in Chinese)

[19] YAO Rui, ZHU Wenbai, HUANG Peng, Accuracy analysis of stewart platform based on interval analysis method[J], *Chinese Journal of Mechanical Engineering*, 2013, 26(1): 29–34.

[20] CHEN Yuzhen, XIE Fugui, LIU Xinjun, et al. Error modeling and sensitivity analysis of a parallel robot with SCARA(Selective compliance assembly robot arm) motions[J]. *Chinese Journal of Mechanical Engineering*, 2014, 27(4): 693–702.

[21] RUGBANI A, SCHREVE K, The kinematics and error modeling of a novel micro-CMM[J]. *The International Journal of Advanced Manufacturing Technology*, 2015, 78(5–8): 961–969.

[22] LEI Yingjie, ZHANG Shanwen. *Genetic algorithm toolbox of MATLAB and its application*[M]. Xi'an: Xidian University Press, 2014. (in Chinese)

[23] National Development and Reform Commission of the People's Republic of China. JB/T 10792.1–2007 The 5-axes simultaneous vertical machining centers-part 1: testing of the accuracy[S]. Beijing: China Machine Press, 2008. (in Chinese)

[24] SUN Tianhui. *Kinematic calibration of a 3-DOF spindle head–A3 head*[D]. Tianjin: Tianjin University, 2011. (in Chinese)

Biographical notes

NI Yanbing, born in 1964, is currently an associate professor at *Tianjin University, China*. He received his PhD degree at *Tianjin University, China*, in 2000. His research interests include parallel robotics and CNC equipment.
Tel: +86+13602126152; E-mail: niyb5812@tju.edu.cn

ZHANG Biao, born in 1991, is currently a master candidate at *School of Mechanical Engineering, Tianjin University, China*. His research interests include accuracy design of parallel mechanisms and error compensation of machine tools.
E-mail: zbiao1991@163.com

SUN Yupeng, born in 1989, is currently an engineer at *China Faw Group Corporation R&D Center.* He received his master degree at *School of Mechanical Engineering, Tianjin University, China*, in 2015. His research interests include mechanism design and parallel robots.
E-mail: 1013347803@qq.com

ZHANG Yuan, born in 1992, is currently a master candidate at *School of Mechanical Engineering, Tianjin University, China*. His research interests include kinematic calibration of parallel mechanisms and robotics.
E-mail: 552308868@qq.com